Since January 2020 Elsevier has created a COVID-19 resource centre with free information in English and Mandarin on the novel coronavirus COVID-19. The COVID-19 resource centre is hosted on Elsevier Connect, the company's public news and information website.

Phytomedicine Plus 2 (2022) 100233

Contents lists available at ScienceDirect

Phytomedicine Plus

journal homepage: www.sciencedirect.com/journal/phytomedicine-plus

In silico, *in vitro* screening of plant extracts for anti-SARS-CoV-2 activity and evaluation of their acute and sub-acute toxicity

Damle Latha [a], Damle Hrishikesh [b], Ganju Shiban [b], C Chandrashekar [a], BR Bharath [a,1,*]

[a] *Computational Biology, Atrimed Biotech LLP, Banglore, 560100, India*
[b] *Atrimed Pharmaceuticals Pvt. Ltd, Banglore, 560001, India*

ARTICLE INFO

Keywords:
Molecular docking
Plant extracts
Cytotoxicity
Anti-SARS-CoV-2
In vivo toxicity

ABSTRACT

Background: In the absence of a specific drug for COVID 19, treatment with plant extracts could be an option worthy of further investigation and has motivated to evaluate the safety and anti-SARS-CoV-2 activity of plant extracts.

Purpose: To screen the phytochemicals for anti-SARS-CoV-2 *in silico* and evaluate their safety and efficacy *in vitro* and *in vivo*.

Method: The phytochemicals for anti-SARS-CoV-2 were screened *in silico* using molecular docking. The hits generated from *in silico* screening were subjected for extraction, isolation and purification. The anti-SARS-CoV-2 activity of *Zanthoxylum piperitum* (E1), *Withania somnifera* (E2), *Calophyllum inophyllum* (E3), *Andrographis paniculata* (E4), *Centella asiatica* (E5) ethanol extracts. The aerial parts were used for E1, E3, E4, E5 and root was used for E2. The *in vitro* safety and anti-SARS-CoV-2 activity of plant methanol extracts were performed in VeroE6 cells using Remdesivir as positive control. The acute and sub-acute toxicity study was performed in Wistar male and female rats.

Results: The percentage of cell viability for E4, E5 and E2 treated VeroE6 cells were remarkably good on the 24th and 48th hour of treatment. The *in vitro* anti-SARS-CoV-2 activity of E4, E5 and E2 were significant for both E gene and N gene. The percentage of SARS-CoV-2 inhibition for E4 was better than Remdesivir. For E gene and N gene, Remdesivir showed IC_{50} of 0.15 μM and 0.11 μM respectively, For E gene and N gene, E4 showed IC_{50} of 1.18 μg and 1.16 μg respectively. Taking the clue from *in vitro* findings, the E4, E5 and E2 were combined (E 4.5.2) and evaluated for acute and sub-acute toxicity in Wistar male and female rats. No statistically significant difference in haematological, biochemical and histopathological parameters were noticed.

Conclusion: The study demonstrated the anti-SARS-CoV-2 activity *in vitro* and safety of plant extracts in both *in vitro* and *in vivo* experimental conditions.

Abbreviations

SARS-CoV-2:	Severe Acute Respiratory Syndrome Coronavirus 2
ZP:	*Zanthoxylum piperitum*
WS:	*Withania somnifera*
CI:	*Calophyllum inophyllum*
AP:	*Andrographis paniculata*
CA:	*Centella asiatica*
HSV:	Herpes simplex virus
HIV:	Human immunodeficiency virus
S-Protein:	Spike glycoprotein
RdRp:	RNA dependant RNA polymerase
Mpro:	Mpro
3CLpro:	3-chymotrypsin like protease
PDB:	Protein Data Bank
OPLS_2005:	Optimized potentials for liquid simulations_2005
EtOAc:	Ethyl acetate
DCM:	Dichloromethane
MeOH:	Methanol
HPLC:	High-performance liquid chromatography
PDA:	Photodiode-Array Detection
UV:	Ultraviolet

* Corresponding author.
E-mail address: bharath.br@atrimed.com (B. Bharath).
[1] Research Head

https://doi.org/10.1016/j.phyplu.2022.100233
Received 27 September 2021; Received in revised form 21 January 2022; Accepted 29 January 2022
Available online 31 January 2022

MRM: Multiple reaction monitoring
N2: Nitrogen
RCBF: Regional centre for biotechnology, Faridabad
DMSO: Dimethylsulfoxide
TS: Test Substance
MOI: Multiplicity of infection
RNA: Ribonucleic acid
qRT-PCR Quantitative reverse transcription-polymerase chain reaction
OECD: Organization for economic cooperation and development
NUCARE Nitte university centre for animal research
AST: Aspartate aminotransferase
ALT: Alanine aminotransferase
ALP: Alkaline phosphatase
TP: Total protein
T.Chol: Total cholesterol
TG: Triglyceride
BUN: Blood urea nitrogen
ANOVA: Analysis of variance
SD: Standard deviation
HTVS: High throughput virtual screening
SP: Standard precision
XP: Extra precision
ACE2: Angiotensin-Converting enzyme 2
RBD: Receptor-Binding domain
RT: Retention time
E gene: Envelope gene
N gene: Nucleoprotein gene
RBC: Red blood cell
PCV: Packed cell volume
MS: Mass spectroscopy
IC_{50}: Half-maximal inhibitory concentration
CT: Cycle threshold

Introduction

Currently, there is no specific drug for SARS-CoV-2 infection. Efforts are being made globally to identify agents for preventive, supportive and therapeutic care. Many plants used in traditional medicine have been reported to have antiviral properties. In the present study, we evaluated cytotoxicity and anti-SARS-CoV-2 activity of *Zanthoxylum piperitum* Benn. (Rutaceae) methanol extract, *Withania somnifera* (L.) Dunal (Solanaceae) methanol extract, *Calophyllum inophyllum* L., (Clusiaceae) methanol extract, *Andrographis paniculata* (Burm.f.) Nees (Acanthaceae) methanol extract and *Centella asiatica* (L.) Urb. (Apiaceae) methanol extract. We also studied animal toxicity for these extracts.

Z. piperitum leaf methanol extracts have been investigated against influenza viruses, A/WS/33, A/PR/8 and B/Lee/40 and reported to have antiviral activity at low concentration of lower than 10 μg/mℓ with no cytotoxicity (50 μg/mℓ) against all of three viruses (Choi et al., 2008). *Z. piperitum* extracts have shown inhibition of human rhinovirus 2, human rhinovirus 3, coxsackie A16 virus, coxsackie B3 virus, coxsackie B4 virus, and enterovirus 71 virus (Choi et al. 2016).

W. somnifera has been extensively studied for its antioxidant, antibacterial, antifungal, anti-inflammatory, and hematopoietic activity. A prospective, randomized double-blind, placebo-controlled study of *W. somnifera* root methanol extract demonstrated its safety and efficacy in reducing stress and anxiety in adults (Chandrasekhar et al., 2012). *W. somnifera* contains pharmacologically active compounds like sitoindosides and alkaloids, which previously showed various biological activities (Bhattacharya and Muruganandam 2003; Kulkarni and Dhir 2008; Provino 2010; Singh et al., 2010; Sharma et al., 2011). *W. somnifera* has been screened for antiviral activity against infectious bursal disease virus replication. The *W. somnifera* hydroalcoholic roots extract showed 99.9% inhibition of the virus at the highest nontoxic concentration (Pant et al., 2012).

The compounds inophyllum B, inophyllum P isolated from *C. inophyllum* were found to have anti-HIV-1 reverse transcriptase activity (Laure et al., 2008). The compound calanolide A from *C. inophyllum* has also been reported to inhibit HIV-1 replication (Kashman et al., 1992).

A. paniculata is a common medicinal plant used in Asian countries to treat various diseases like pharyngitis, tonsillitis, upper respiratory tract infection and acute monocytic leukaemia (Saxena et al., 2010; Tan et al., 2017; Thamlikitkul et al., 1991). Preparations containing *A. paniculata* extract reported to prevent and improve the symptoms of common cold (Saxena et al., 2010). The therapeutic effect of *A. paniculata* in common cold management has been demonstrated by several clinical trials over the past 30 years (Caceres et al., 1997; Melchior et al., 1997; Melchior et al., 2000; Thamlikitkul et al., 1991). The meta-analysis studies have also endorsed the same (Poolsup et al., 2004).

C. asiatica has been used in the Ayurvedic tradition of India and listed in an ancient Indian medical text called 'Sushruta Samhita' (Chopra et al., 1986; Diwan et al., 1991). *C. asiatica* is also used in Indonesian islands. The primary active constituents of *C. asiatica* are triterpenoids, which include asiaticosides, madecassoside and madasiatic acid (Singh and Rastogi 1961). *C. asiatica* in combination with *Maclura cochinchinensis* (Lour.) Corner (Moraceae) and *Mangifera indica* L. (Anacardiaceae) was evaluated for anti-herpes simplex virus (HSV) activity and treatment for muco-cutaneous HSV infection (Yoosook et al., 2000).

The anti-SARS-CoV-2 activity of plant extracts and their components was evaluated by many researchers worldwide. However, in the present study efforts have been made to screen the phytochemicals for anti-SARS-CoV-2 *in silico* and evaluate their safety and efficacy *in vitro* and *in vivo*.

Materials and methods

Virtual screening of plant molecules against SARS-CoV-2 targets

Ligand preparation

Considering the availability and sustainability of medicinal plants, 521 Indian medicinal plants were identified and the structure of phytochemicals from each plant were manually curated from a reported research articles of high quality (Locally hosted database at Atrimed). The biological active conformations of 13,105 curated plant molecules were obtained through ligand preparation process. The structure of plant molecules were sketched using a 2D sketcher tool available in Schrodinger maestro and subjected for ligand minimisation using Ligprep (Version 2.3, Schrödinger, LLC, New York, 2009). During the minimisation, force field OPLS_2005 were assigned and stereoisomers were calculated after retaining specific chiralities.

Protein preparation

The proteins involved in, entry, replication and assembly of SARS-CoV-2 in human host such as Spike glycoprotein (S-Protein), RNA dependant RNA polymerase (RdRp), Main protease (Mpro), and 3-chymotrypsin like protease (3CLpro) were identified as potential drug targets (Bharath et al. 2020; Douangamath et al., 2020; Jin et al., 2020; Yin et al., 2020). The structure of S-Protein was modelled as reported in Bharath et al. 2020 and the structure of remaining target proteins were downloaded from Protein Data Bank (PDB). The three-dimensional structure of target proteins were prepared using the protein preparation wizard workflow available in the Schrödinger 2019–2 glide module. During the protein preparation, the crystallographic water molecules with less than three H-bonds were deleted and hydrogen atoms corresponding to neutral pH were added in consideration of ionisation states of amino acids. Following this, coordinates for any missing side-chain atoms were added using Prime v4.0, Schrödinger 2019–2 and energy minimisation was performed using the OPLS_2005 force field.

Virtual screening

The active site on the prepared receptor was confined with a 10 Å

radius by centring around selected residues (Receptor Binding Domain (Leu464, Phe495, and Ser503)) for S-Protein and centring co-crystal molecules (RdRp: Triphosphate form of Remdesivir (RTP) and Mpro: Inhibitor N3) for other target proteins. This generated a grid box measuring 20 × 20 × 20 Å. The docking of phytochemicals over target proteins was performed using Glide v7.8. Schrödinger 2019–2 in different modes sequentially with defined and incremental precision, and computational time differences. The phytochemicals with best docked conformer and minimum glide energy were shortlisted for the evaluation of *in vitro* anti-SARS-CoV-2 activity.

Extraction, isolation and purification of plant molecules

Plant materials, chemicals and reagents

The aerial parts of *Z. piperitum, C. inophyllum,A. paniculata* and *C. asiatica,* and root of *W. somnifera* were procured from Herbo Ayurvedics, Calicut, Kerala, India and authenticated by using herbarium, maintained in our laboratory (Voucher No: SDMAR307, SDMAR290, SDMGH165, SDMGH047 and SDMGH083). The Organic solvents such as hexane, EtOAc; DCM, MeOH, and Silica gel (60–120 mesh) for sample preparation were procured by Avra Synthesis Pvt Ltd. Silica high performance Gold columns were purchased from Redi sepRf, Teledyne ISCO. Solvents for HPLC, HPLC-grade acetonitrile; water and MeOH were procured from Sigma- Aldrich.

Extraction and primary analysis of crude extracts

The plant material (500 g) was packed in Soxhlet extractor, defatted by using hexane for about four h. The dried defatted plant material was again extracted with 3l of 100% MeOH. The total extract was then concentrated by rotary evaporation under vacuum to obtain the ethanol crude extracts. The 0.1 g of crude extracts were dissolved in 10 ml of MeOH and subjected to thin layer chromatography using silica gel as stationary phase and different sets of solvent system as mobile phase.

Liquid chromatography–mass spectrometry (LC-MS) based separation and purification

The crude extracts were subjected for flash chromatography (Teledyne ISCO, CombiFlash NEXTGEN 300 system) using Redisep C-18 86 G column for semi purification. Acetonitrile, water, and MeOH were the solvents used at different concentrations. The semi purified fractions were further subjected to HPLC for next level purification. The HPLC system used was WatersTM e2695 consisting of a quaternary pump, an automatic degasser, and an auto-sampler, having PDA and UV detector, column used was Shimpack C-18 (ODS) (250 mm*4.6, 5 μm) column. The molecular weight of purified fractions were identified using the Shimadzu2020 LC- MS system. The temperature of the column was set to 40 °C and a 5 μl aliquot of the sample solution was injected at specific flow rate vis., 0.3 ml/min, 1 ml/min, 1 ml/min, 1 ml/min, and 0.3 ml/min for *W. somnifera, C. inophyllum, A. paniculata* and *C. asiatica* fractions respectively. The gradient system followed for each sample was 70:30 for water: acetonitrile, 100% for acetonitrile, and 70:30 for 0.1% formic acid in water: 0.1% formic acid in MeOH. The positive ionization mode was used for compound ionization. The quantification was obtained in multiple reaction monitoring (MRM) mode with the precursor-product ion transition. High-purity nitrogen (N_2) was used as the nebulizing gas, and nitrogen (N_2) was used as the drying gas at a flow rate of 15 l/min. The mass spectrometer was operated at a capillary voltage of 4000 V, source temperature of 100 °C and desolvation temperature of 350 °C.

Before sending the pure fractions for *in vitro* studies, they were allotted code names:*Z. piperitum* as E1, *W. somnifera* as E2, *C. inophyllum* as E3, *A. paniculata* as E4, *C. asiatica* as E5. The *in vitro* antti-SARS-CoV-2 activity was carried out at regional centre for biotechnology, Faridabad (RCBF).

In vitro cytotoxicity and anti-SARS-CoV-2 activity

In *in vitro* cytotoxicity and anti-SARS-CoV-2 activity was carried out at RCBF, using the methods described below:

Preparation of cells

The cytotoxicity assay was done in a 96-well plate, with 3 wells for each sample. 1 × 10e4 VeroE6 cells were plated *per* well and incubated at 37 °C overnight for the monolayer formation. Next day, cells were incubated with 1 μl of extract in 200 μl of 0.5% dimethyl sulfoxide (DMSO). The concentration of Remdesevir, E1, E2, E3, E4 and E5 methanol extracts were 10, 30, 2.8, 5, 5.5, and 45 mg/ml respectively. The control cells were incubated without test sample (TS).

In vitro cytotoxicity

The treated incubated cells were collected at 24 and 48 h and stained with Hoechst 33,342 and Sytox orange dye. Sixteen images *per* well were taken at 10x, which covered 90% of well area using Image Xpress Microconfocal (Molecular Devices, USA). The percentage of cell viability was measured by counting the number of dead cells in the Sytox image as described by Tan et al., 2004.

In vitro anti-SARS-CoV-2 activity

The prepared cells were infected with SARS-CoV2 at a multiplicity of infection (MOI) of 0.01. After 24 and 48 h, viral RNA was extracted from 100 μl culture supernatant and subjected to qRT-PCR where Ct values for N and E gene sequence were determined. Inhibition of virus replication was determined by the Ct value in TS-treated cells compared to the control. Remdesivir was used as a positive control for viral inhibition (Caly et al. 2020).

In vitro IC_{50} determination

The prepared cells were incubated with TS at seven different concentrations as follows. The concentrations used for E4, were 5.5, 2.75, 1.37, 0.68, 0.34, 0.17 and 0.08 μg. The concentrations used for Remdesivir were 10, 3, 1, 0.3, 0.1, 0.03 and 0.01 μM. The control cells were incubated with 0.5% DMSO.

The cells were infected with SARS-CoV2 at a MOI of 0.01 and after 48 h, viral RNA was extracted from 100 μl culture supernatant and subjected to qRT-PCR. The Ct values for N and E gene sequence were recorded and the inhibition of virus replication was determined based on the change in the Ct value in TS-treated cells compared to the control. IC_{50} values were determined using AAT Bioquest IC_{50} calculator.

In vivo acute and subacute toxicity

Experimental animals

Toxicity assays were conducted in accordance with the standard guidelines of the organization for economic cooperation and development (OECD, 2001) for use of animals in scientific research. Experimental animals were housed in groups of three for acute toxicity study and a group of six animals for sub-acute toxicity study as *per* standard laboratory conditions.

The experimental female rats were bred and reared at the animal care facility in NUCARE, Nitte University, Mangalore and experiments were carried out in the same facility. Adult albino wistar non-pregnant female rats weighing 200−220 g and between 8 and 10 weeks of age were used.

Preparation of dose formulation

The test substance was prepared by standard procedure. Extracts weighing 833.33 mg E2, E4 and E5 each were placed in a mortar. Small quantity of water was added, and the sample was triturated using a pestle. Once all samples were wet, the water was added slowly to make up the total volume to 5 ml, while trituration continued to get simple suspension and the dose formula was labelled as E 4.5.2.

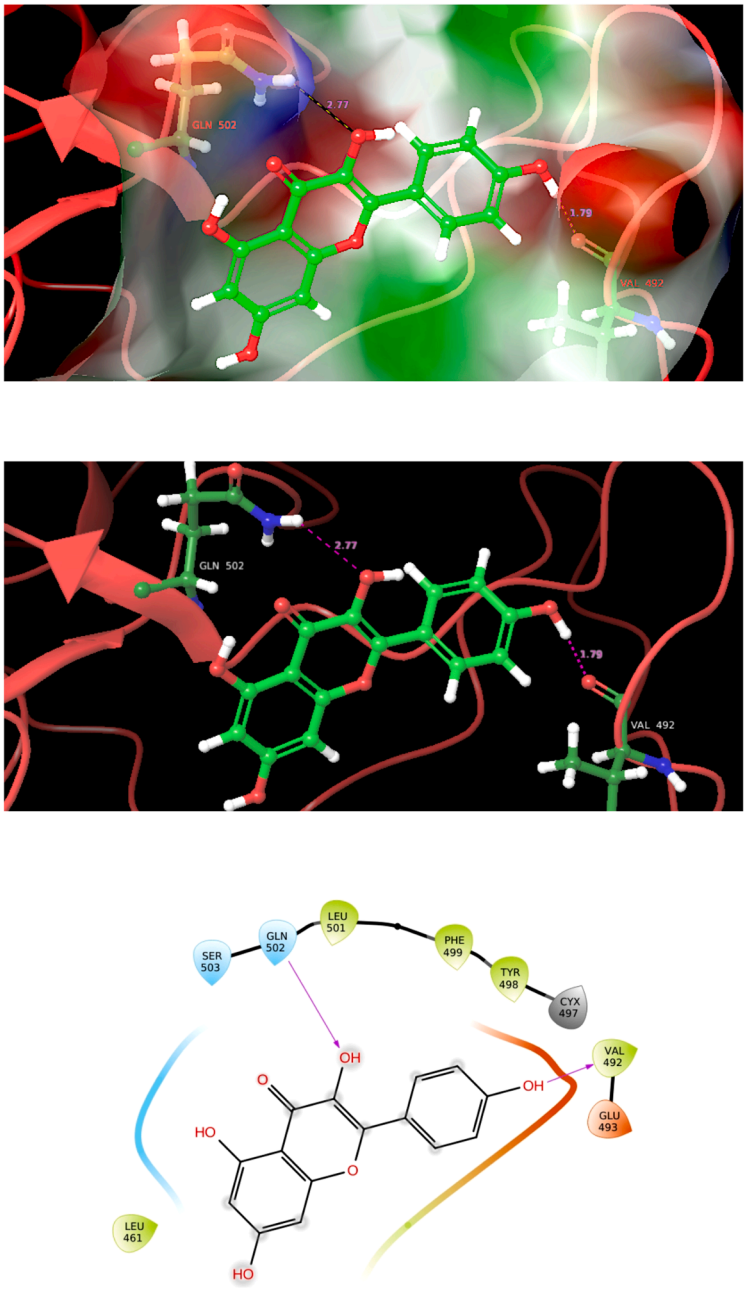

Fig. 1. Molecular docking of Kaempferol (Green coloured ball and stick) in the RBD site of SARS-CoV-2 S-Pro-tein (Homology model, Bharath et al. 2020). **A:** Three dimensional view where receptor is rendered with molecular surface to illustrate the interaction of kaempferol with the amino acids Gln502 and Val492 making the ridges which are sterically complementary to the cleft on human ACE2 receptor. **B:** 3D view illustrating the interaction of kaempferol hydroxyl groups with Nγ of Gln502 side chain and ketone group of Val492 back bone residues. **C:** The protein ligand interaction diagram illustrating the interaction of kaempferol in the RBD site of SARS-CoV-2 S-Pro-tein; the grey highlights on ligand molecules represents solvent exposure.

Acute toxicity study

Animals were fasted overnight (12 h) but had free access to water. The single dose of E 4.5.2 at 2000 mg/kg was administered using an oral gavage needle. Animals were observed every 30 min for the first 4 h, and daily thereafter, for a total of 14 days for toxic manifestations by observing clinical signs (salivation, excitability, draping, tremors, twitching, rising fur) and death. The weight and food consumption of the experimental animals were recorded on the first day and 14th day. After 14 days, they were sacrificed.

Subacute toxicity study

As *per* OECD (2001) recommendations, the dose at which the extract is not expected to produce mortality or severe acute toxicity is called the starting dose of the sub-acute toxicity (Tilahun et al., 2020).

The 2000 mg/kg body weight of the E 4.5.2 was the highest dose. A total of 72 Wistar male and female rats were divided into 6 groups; each group consisted of 6 male and 6 female rats. The groups five and six were called satellite groups. Each group was given 1 ml/100 g of body weight of E 4.5.2 at concentrations of 0 mg/kg (control), 200 mg/kg (low dose), 400 mg/kg (medium dose), 800 mg/kg (high dose), 0 mg/kg (control reversal) and 800 mg/kg (high dose reversal). All the six groups received the treatment for 28 days.The weight and food consumption of animals were measured weekly till the 28th day. On day 29, control, low, medium and high dose groups were sacrificed. The satellite groups were maintained for another 14 days without any treatment to observe the reversible untoward effect of treatment if any.On day 43, satellite groups were sacrificed for haematological, biochemical and histopathological examinations.

- *Haematological studies*

1 ml of blood samples were collected from each rat. The haematological examination was carried out to measure differences in Red Blood Cell (RBC), Packed cell volume (PCV), Haemoglobin, Neutrophils,

Table 1
List of hits generated by molecular docking of phytochemicals against three major SARS-CoV-2 targets.

Phytochemical	Plant Source	Target	No. of H-Bonds	H-Bond forming Atoms Ligand	Target	Bond length in Å	Docking Energy mg/mol
Kaempferol	*C. asiatica*	S-Protein	2	C4`: OH	Val492: O	1.79	-5.21
				C7: OH	Gln502: Nγ	2.77	
Andrographidine C	*A. paniculata*	RdRp	5	C2``: OH	U20: C3:OH	2.49	-8.12
				C4: O	U20: C3:OH	2.16	
				C6``: OH	Lys551: Hζ1	2.33	
				C4``: OH	Glu811: Oε2	2.47	
				C6``: OH	POP 1003: O2	2.63	
Coagulin G	*W. somnifera*	MPro	3	C17: OH	Thr26: O	2.04	-9.17
				C3: OH	Ser144: Hγ	2.39	
				C1: O	His163: Nε2	2.55	
Zanthoxyl flavone	*Z. piperitum*	MPro	4	C5: OH	Thr26: O	1.96	8.23
				O	Gly143: N	3.71	
				C4`: OH	His163: Nε2	2.02	
				C3: OH	Gln189: Oε1	2.73	
3,4,6,8-Tetrahydroxy-7-(3- hydroxy-3-methylbutyl)−9H-xan- thene-9-one	*C. inophyllum*	MPro	3	C11:OH	Thr25: Oγ1	1.81	8.75
				C6: OH	Thr26: O	2.28	
				C3: OH	His163: Nε2	1.80	

Basophils, Lymphocytes and Monocytes counts.

- *Biochemical markers*

The levels of glucose, Aspartate aminotransferase (AST), Alanine aminotransferase (ALT), Alkaline phosphatase (ALP), Total Protein (TP), Albumin, Total cholesterol (T.Chol), Triglyceride (TG), Blood urea nitrogen (BUN), creatinine, total bilirubin, calcium, phosphate, sodium and potassium were measured.

- *Histopathological examinations*

All rats were sacrificed using Isoflurane anaesthesia at the end of the 14th day for acute toxicity and at the end of the 28th day for sub-acute toxicity studies. Macroscopic and histopathological examinations were done for liver, kidney and jejunum.

Statistical analysis

The data were analysed using Graph Pad Prism version 6 Software. For each group, one way ANOVA analysis was done followed by Dunnett's comparison test. The data were expressed as mean ± standard deviation (SD). A p-value < 0.05 was considered as statistically significant.

Results and discussion

Virtual screening

The virtual screening of 13,105 phytochemicals at different precision levels like high throughput virtual screening (HTVS), standard precision (SP) and extra precision (XP) has suggested the interaction of phytochemicals from *Z. piperitum, W. somnifera, C. inophyllum, A. paniculata* and *C. asiatica* with SARS-CoV-2 drug targets.

The SARS-CoV-2 enters the host by interacting its S-Protein with a host receptor called ACE2. The S-protein consists of two subunits, S1 as the receptor-binding domain (RBD) and S2 subunit as the fusion protein. The residues forming RBD of SARS-CoV-2 Leu455, Phe486, and Ser494 (corresponding to Leu464, Phe495, and Ser503 of S-protein of SARS-CoV-2, modelled in our earlier study (Bharath et al. 2020)), are and reported to play a critical role in disease transmission (Wan et al., 2020). SARS-CoV-2 recognises human ACE2 by its residues Gln493 and Leu455 (corresponds to Gln502 and Leu464), thereby enhancing viral binding to human ACE2. Hence, the interaction of phytochemicals with Gln502 or Leu464 can inhibit the interaction of S-Protein with the ACE2 receptor and stop the entry of SARS-CoV-2 into the host cell. The molecular docking has shown the interaction of kaempferol from *C. asiatica* with the residues Gln502 and Val492 making the ridges, which are sterically complementary to the cleft on the human ACE2 receptor (Fig. 1A). The H-bonds formed between hydroxyl groups of kaempferol and Nγ of Gln502 side chain and ketone group of Val492 backbone residues showed strong interaction (Fig. 1B). The major contribution for docking energy was contributed by H-Bonds (Table 1) and the penalty was due to high solvent exposure of kaempferol on the surface of S-Protein (Fig. 1C).

The inhibition of SARS-CoV-2 replication in cell-based assays are demonstrated for small molecule antiviral nucleoside analogue drugs like Remdesivir, Favipiravir, Ribavirin, and Galidesivir (Lu et al. 2020; Sheahan et al. 2020). The nucleotide analogue drugs are reported to inhibit the viral enzyme called RdRp through non-obligate RNA chain termination mechanism, and the crystal structure of the template-RTP RdRp complex provides an experimental model to rationalise how these drugs inhibit the SARS-CoV-2 RdRp activity. In the present study, the conformation of andrographidine C from *A. paniculata* has also shown non-obligate RNA chain termination type of interaction (Fig. 2) and the interaction was similar to the co-crystal (Fig. 2D). The orientation of andrographidine C was parallel to the base Uracil 20 (U 20) of RNA and the interaction was found stable due to π-π stacking between coumarin moiety and Uracil base. Additionally, the H-Bonds formed by electron donating hydroxyl groups present in andrographidine C have strengthened the interaction with minimum docking energy (Table 1).

Jin et al. have elucidated the inhibitory mechanism of N3 by determining the crystal structure of SARS-CoV-2 Mpro in complex with N3 (Jin et al., 2020). The elucidated crystal structure is a homodimer with two designated protomers A and B. The specific interactions of N3 with Mpro showed the covalent bond between Sγ atom of Cys145 and Cβ atom of the vinyl group in N3. The side chains of Phe140, Asn142, Glu166, His163 and His172 of protomer A, and the backbone atoms of Phe140 and Leu141 of protomer A are involved in the formation of the S1 subsite. The lactam at P1 of N3 inserts into the S1 subsite and forms a hydrogen bond with His163 of protomer A. Similarly, coagulin G from *W. somnifera*, zanthoxyl flavone from *Z. piperitum* and 3,4,6,8-Tetrahydroxy-7-(3-hydroxy-3-methylbutyl)−9H-xanthen-9-one from *C. inophyllum* showed interaction with His163 (Fig. 3, 4 and 5). The interactions were favoured by other residues in the cleft (Table 1).

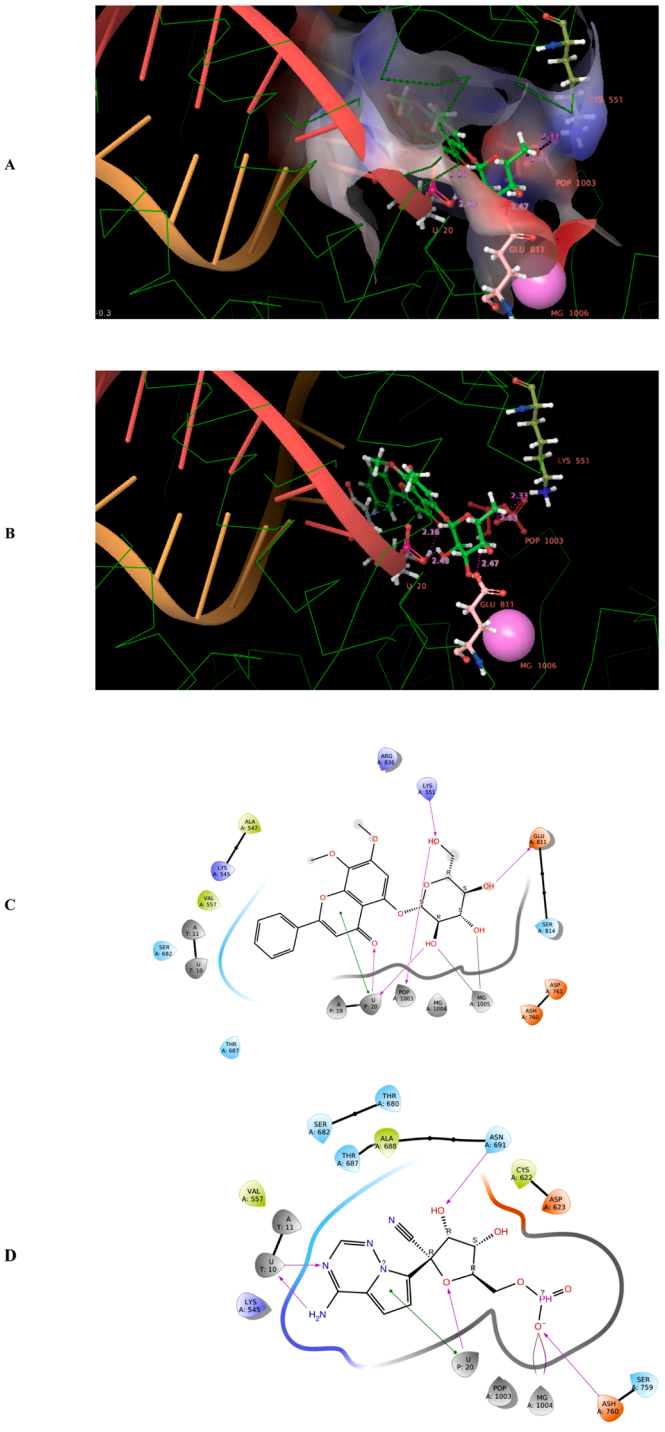

Fig. 2. Molecular docking of andrographidine C (Green coloured ball and stick) in the RNA binding site of SARS-CoV-2 RdRp (PDB ID: 7BV2) **A:** Three dimensional view where RDRP RNA binding site is rendered with molecular surface to illustrate the interaction of andrographidine C with the amino acids Lys551and Glu811; non-obligate RNA chain termination due to interaction with Uracil 20 is also notable. **B:** 3D view illustrating the H-bonds between hydroxyl groups of andrographidine C and ribose group of U20, Oε2 of Glu811 and Hζ1 of Lys551; the pi-pi stacking (blue dotted line) between coumarin group of andrographidine C and Uracil 20 is no-Table. **C:** The protein ligand interaction diagram illustrating the interaction of andrographidine C in the RNA bind-ing site of SARS-CoV-2 RdRp. **D:** The protein ligand interaction diagram illus-trating the interaction of the co-crys-tal RTP in the RNA binding site of SARS-CoV-2 RdRp; the grey highlights on ligand molecules represents sol-vent exposure.

Extraction, isolation and purification of plant molecules

The fractions of interest were purified using flash chromatography and confirmed for the presence of zanthoxyl flavone, coagulin G, 3,4,6,8-Tetrahydroxy-7-(3-hydroxy-3-methylbutyl)−9H- xanthen-9-one, andrographidine C, and kaempferol in *Z. piperitum, W. somnifera, C. inophyllum, A. paniculata* and *C. asiatica* MeOH extracts respectively.

The flash chromatographic fractionation of crude MeOH extracts of *Z. piperitum* has led to four different polarity fractions at different RT (**Table S1**). The HPLC chromatogram for the first fraction obtained from flash chromatography at Rt1 of 25 min has shown a high resolution peak at the retention time of 6.4 min based on UV wavelength at 210 nm . The HPLC fraction obtained at the retention time of 6.4 min has shown a peak corresponding 347 *m/z* in MS spectra has ensured the presence of zanthoxyl flavone in *Z. piperitum* MeOH extract. Hence, it is inferred that, zanthoxyl flavone in the extract can interact with Mpro of SARS-CoV-2 and could be responsible for the anti-SARS-CoV-2 activity.

The flash chromatographic fractionation of crude MeOH extracts of *W. somnifera* has led to three different polarity fractions at different RT (**Table S1**). The HPLC chromatogram for the first fraction obtained from flash chromatography at Rt1 of 22 min has shown a high resolution peak at the retention time of 5.2 min based on UV wavelength at 254 nm. The HPLC fraction obtained at the retention time of 5.42 min has shown a peak corresponding 465 *m/z* in MS spectra has confirmed the presence of coagulin G in *W. somnifera* MeOH extract. Hence, it is inferred that, coagulin G in the extract can interact with Mpro of SARS-CoV-2 and could be responsible for the anti-SARS-CoV-2 activity.

The flash chromatographic fractionation of crude MeOH extracts of *C. inophyllum* has led to three different polarity fractions at different RT (**Table S1**). The HPLC chromatogram for the second fraction obtained from flash chromatography at Rt2 of 40 min has shown a high resolution peak at the retention time of 13.8 min based on UV wavelength at 254 nm. The HPLC fraction obtained at the retention time of 13.8 min has shown a peak corresponding 344 *m/z* in MS spectra has confirmed the presence of 3,4,6,8-Tetrahydroxy-7-(3-hydroxy-3-methylbutyl)−9H-xanthene-9-one in *C. inophyllum* methanol extract. Hence, it is inferred that, the 3,4,6,8-Tetrahydroxy-7-(3-hydroxy-3-methylbutyl)−9H-xanthen-9-one in the extract can interact with Mpro of SARS-CoV-2 and could be responsible for the anti-SARS-CoV-2 activity.

The flash chromatographic fractionation of crude MeOH extracts of *A. paniculata* has led to two different polarity fractions at different RT (**Table S1**). The HPLC chromatogram for the second fraction obtained from flash chromatography at Rt2 of 25 min has shown a high resolution peak at the retention time of 6.5 min based on UV wavelength at 210 nm. The HPLC fraction obtained at the retention time of 6.5 min has shown a peak corresponding 463 *m/z* in MS spectra has confirmed the presence of andrographidine C in *A. paniculata* MeOH extract. Hence, it is inferred that andrographidine C in the extract can interact with RdRp of SARS-CoV-2 and could be responsible for the anti-SARS-CoV-2 activity.

The flash chromatographic fractionation of crude MeOH extracts of *C. asiatica* has led to four different polarity fractions at different RT (**Table S1**). The HPLC chromatogram for the second fraction obtained from flash chromatography at Rt2 of 30 min has shown a high resolution peak at the retention time of 8.71 min based on UV wavelength at 370 nm. The HPLC fraction obtained at the retention time of 8.71 min has shown a peak corresponding 290 *m/z* in MS spectra has confirmed the presence of kaempferol C in *C. asiatica* MeOH extract. Hence, it is inferred that, kaempferol in the extract can interact with S-Protein of SARS-CoV-2 and could be responsible for the anti-SARS-CoV-2 activity.

In vitro cytotoxicity

The extracts E3, E4 and E5 showed promotion of VeroE6 cell growth with 110.31%, 103.31% and 106.59% cell viability at 24 h post treatment respectively. E3, E4 and E5 showed 88.72%, 83.53% and 94.48%

A

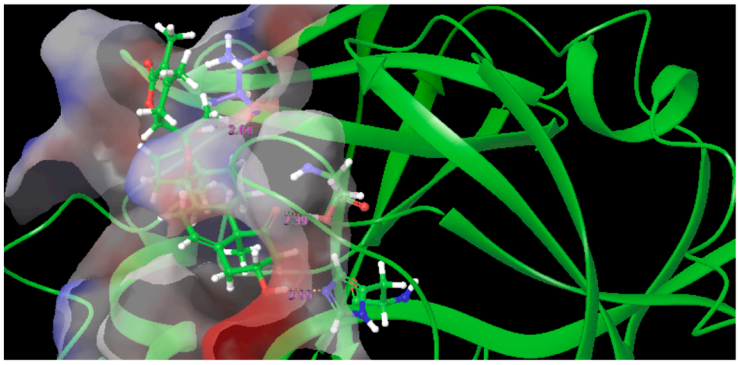

B

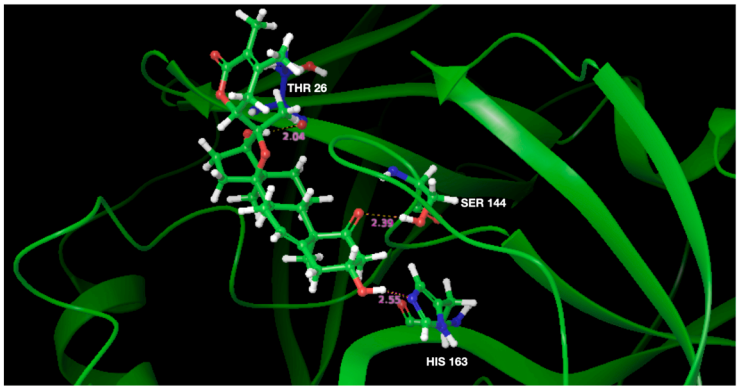

C

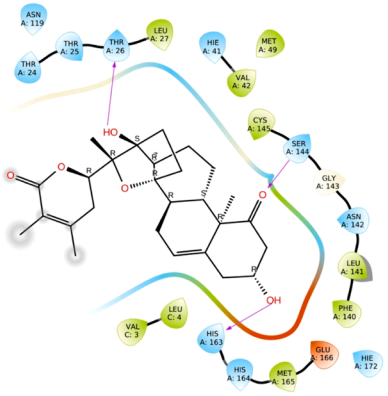

Fig. 3. Molecular docking of coagulin G from *W. somnifera* (Green coloured ball and stick) in the S1 subsite of SARS-CoV-2 MPro (PDB ID: 6LU7). **A:** Three dimensional view where receptor is rendered with molecular sur-face to illustrate the interaction of coagulin G in the S1 subsite. **B:** 3D view illustrating the interaction of coag-ulin G hydroxyl groups with Nε2 of His163, Hγ of Ser144 side chains and ketone back bone atom of Thr26 . **C:** The protein ligand interaction diagram illustrating the interaction of coagulin G in the S1 subsite of SARS-CoV-2 MPro; the grey highlights on ligand molecules represents solvent exposure.

of cell viability at 48 h post treatment.The extracts E1 and E2 showed 88.75% and 77.05%, 85.35% and 88.11% of cell viability at 24 h and 48 h post treatment respectively. Remdesivir at 10 μM concentration showed 99.23% and 94.37% cell viability at 24 and 48 h respectively as shown in Fig. 6. TS showed greater cell viability after 48 h of treatment as compared to Remdesivir.

In vitro anti-SARS-CoV-2 activity

For E gene, at 24 h, Remdesevir, E1, E2, E3, E4 and E5 showed82.28%, 47.86%, 45.93%, −31.50%, 73.54%, and 74.75% inhibition respectively. For the N gene, the inhibition was 80.35%, 49.50%, 45.47%, −19.20%, 71.95%, 74.50% respectively (Fig. 7).

For E gene, at 48 h, Remdesevir, E1, E2, E3, E4 and E5 showed 99.80%,91.30%, 95.60%, 71.72%, 99.90% and 92.07% inhibition. For the N gene, the inhibition was 99.89%, 81.14%, 91.50%, 55.90%, 99.80% and 84.64% respectively (Fig. 8).

Considering the outcomes of *in vitro* anti-SARS-CoV-2 activity, the IC_{50} to inhibit the replication of SARS-COV-2 for each extract (E2, E4 and E5) was determined.

In vitro IC_{50} determination

The concentration-response curves were obtained using seven different concentrations of Remdesivir, E2, E4, and E5. For E gene and N gene, Remdesivir showed IC_{50} of 0.15 μM and 0.11 μM respectively (Fig. 9A**)**, For E gene and N gene, E4 showed IC_{50} of 1.18 μg and 1.16 μg respectively (Fig. 9B**)**. Remdesivir and E4 showed significant delta CT for both E and N genes as shown in Table 2. The Delta CT of E2 and E5 were moderate. In IC_{50} estimation, E2 and E5 did not show consistent CT values, which is common to see in replication of experiments (Vaux et al., 2012). However, the anti-SARS-CoV2 activity of E2 and E5 were significant. The antiviral activity of *W. somnifera* (E2) and *C. asiatica* (E5) has also been reported by earlier researchers on other viruses besides SARS-CoV-2(Kashyap et al., 2020; Sun et al., 2020).

There is a consensus amongst virologists that combining two or more

A

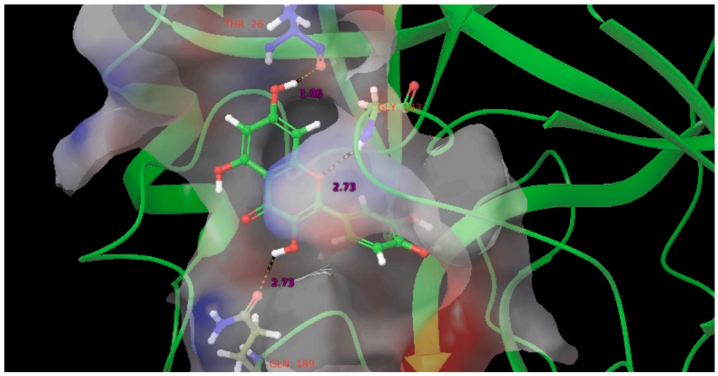

B

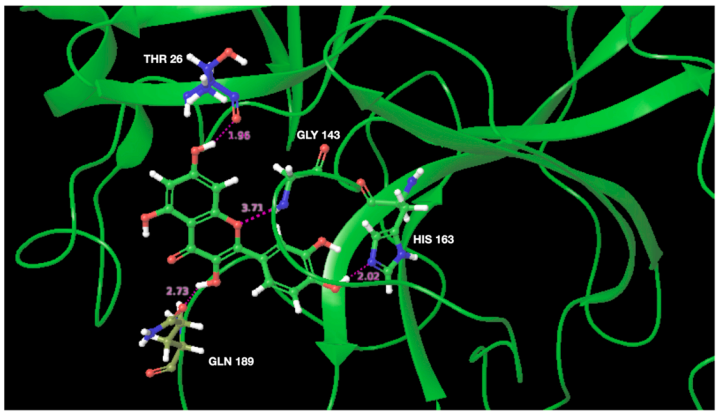

C

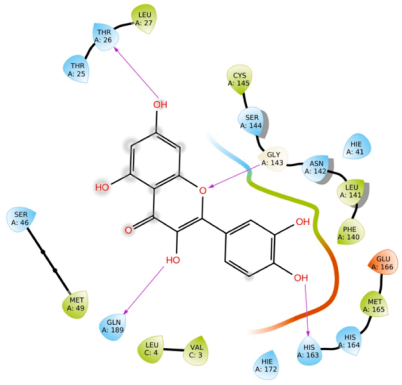

Fig. 4. Molecular docking of zanthoxyl flavone from *Z. piperitum* (Green coloured ball and stick) in the S1 subsite of SARS-CoV-2 MPro (PDB ID: 6LU7). **A:** Three dimensional view where receptor is rendered with molec-ular surface to illustrate the interaction of zanthoxyl flavone in the S1 subsite. **B:** 3D view illustrating the H-Bond formed between zanthoxyl flavone hydroxyl groups and Nε2 of His163, Oε1 of Gln189 side chains and ketone back bone atom of Thr26; O, the member of heterocyclic ring in the coumarin group of zanthoxyl flavone formed the H-Bond with amine back bone atom of Gly143. **C:** The protein ligand interaction diagram illustrating the interaction of zanthoxyl flavone in the S1 subsite of SARS-CoV-2 MPro; the grey highlights on ligand molecules represents solvent exposure.

therapeutic agents with antiviral activity could result in improved antiviral response (Richman et al. 2016; Balkrishna et al., 2021). We therefore decided to evaluate the *in vivo* toxicity of combined extracts of E2, E4 and E5 (E 4.5.2).

In vivo toxicity

Acute toxicity

No abnormalities were observed in clinical signs. Body weights of each animal were recorded prior to the administration of E 4.5.2 (Day 0) and at the end of the experiment (Day 15). The highest dose of E 4.5.2 2000 mg/kg body weight did not induce acute toxicity in rats during the study and the E 4.5.2 fed animals showed healthy growth during the observation period.

Sub-acute toxicity

During the study period, clinical signs of all treated animals were found normal. The food intake and body weights increased proportionately.

Haematological analysis. The administrations of E 4.5.2 in high dose showed increase in RBC and reticulocyte count in both male ($8.707 \times 10^6/mm^3$ cells) and female ($7.278 \times 10^6/mm^3$) compared with the control ($4.75 \times 10^6/mm^3$) however it was not statistically significant (Fig. 10A and Fig. 10B).

PCV, platelet count and eosinophil count in male (low dose: 1.16×10^3/ml and medium dose: 1.16×10^3/ml) and female (low dose: 3.50×10^3/ml and medium dose: 2.33×10^3/ml) animals showed statistically significant ($p<0.05$) decrease compared to control group (Fig. 10A and Fig. 10B). Rest of the haematological parameters (Haemoglobin, Neutrophils, Basophils, Lymphocytes and Monocytes) showed no change (Fig. 10A and Fig. 10B).

Biochemical analysis. Biochemical analysis was conducted on day 29 and

A

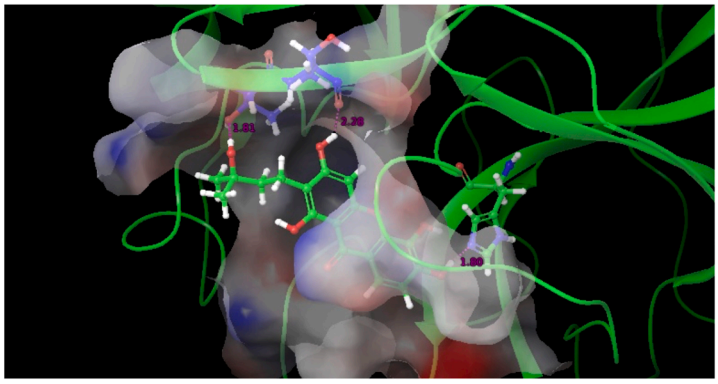

B

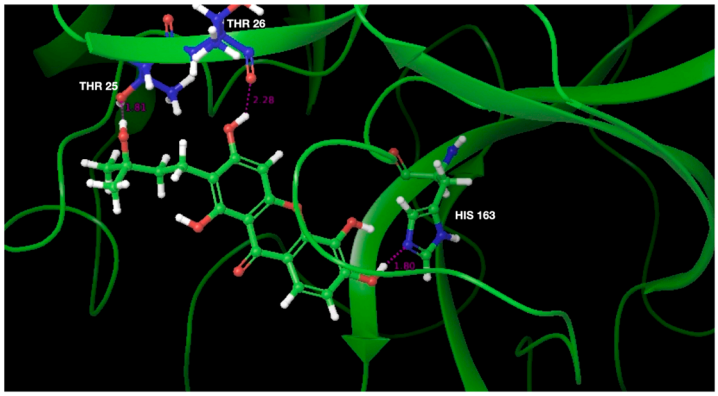

Fig. 5. Molecular docking of 3,4,6,8-Tetrahydroxy-7-(3-hydroxy-3-methylbutyl)−9H-xanthene-9-one from *C. inophyllum* (Green coloured ball and stick) in the S1 subsite of SARS-CoV-2 MPro (PDB ID: 6LU7). **A:** Three dimensional view where receptor is rendered with molecular surface to illustrate the interaction of 3,4,6,8-Tetrahy-droxy- 7-(3-hydroxy-3-methylbutyl)−9H-xanthene-9-one in the S1 subsite. **B:** 3D view illustrating the H-Bond formed between 3,4,6,8-Tetrahydroxy-7-(3-hydroxy-3-methylbutyl)−9H-xanthene-9-one hydroxyl groups and Nε2 of His163, Oγ1 of Thr25 side chains and ketone back bone atom of Thr26. **C:** The protein ligand interaction diagram illustrating the interaction of 3,4,6,8-Tetrahydroxy-7-(3-hydroxy-3-methylbutyl)−9H-xanthene-9-one in the S1 subsite of SARS-CoV-2 MPro; the grey highlights on ligand molecules represents solvent exposure.

C

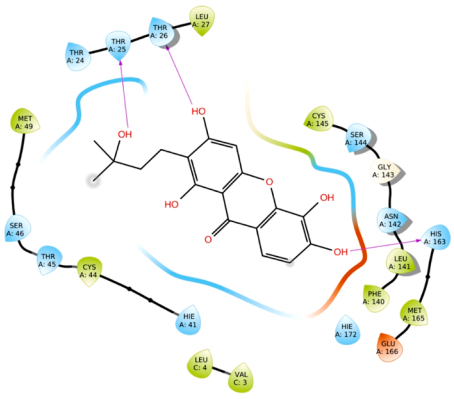

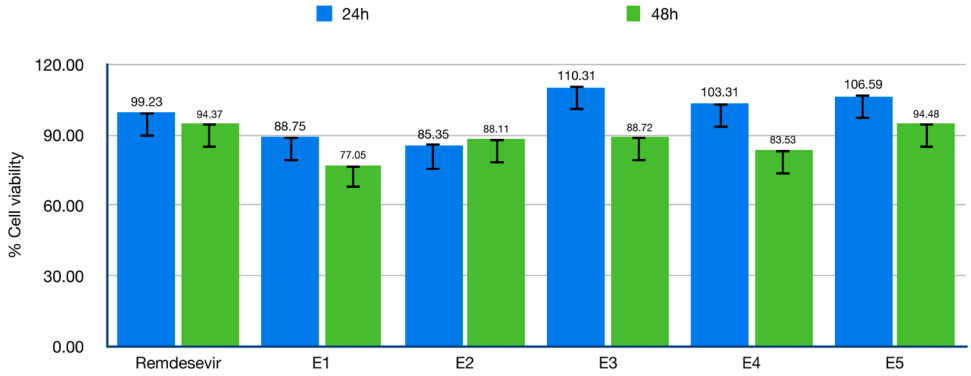

Fig. 6. The viability of VeroE6 cells treated with plant extracts and Remdesevir for 24 and 48 h.

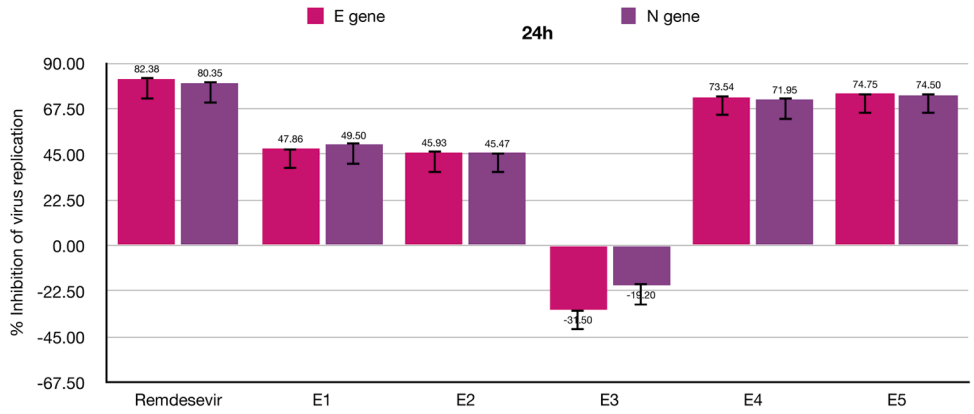

Fig. 7. Percentage inhibition of SARS-CoV-2 replication by Remdesevir and TSs after 24 h of treatment considering the replication of E and N genes.

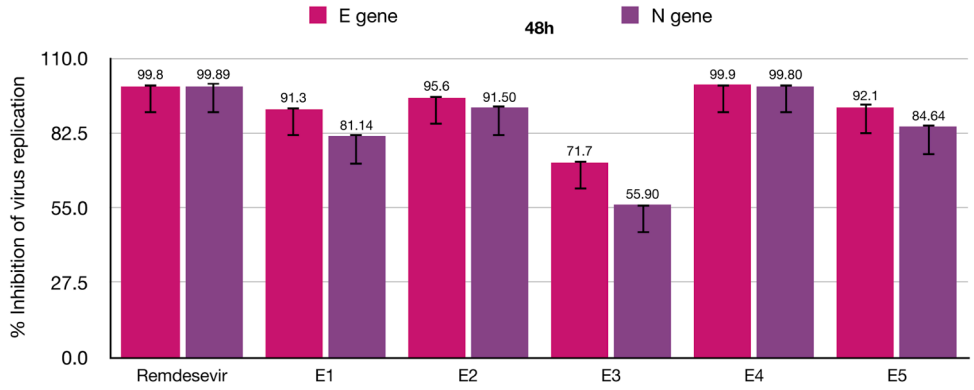

Fig. 8. Percentage inhibition of SARS-CoV-2 replication by Remdesevir and TSs after 48 h of treatment considering the replication of E and N genes.

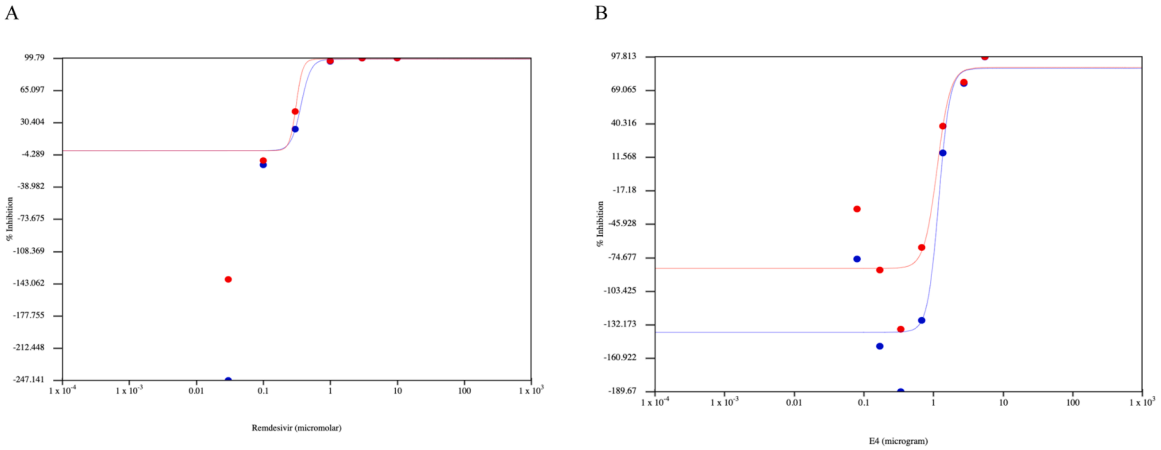

Fig. 9. (A) Concentration dependant response of Remdesivir for SARS-CoV-2 E gene (Blue) and N gene (Red) **(B)** Concentration dependant response of ATRI-CoV-E4 for SARS-CoV-2 E gene (Blue) and N gene (Red).

43; the following observations were made by comparing with control groups.

- *Glucose*

The male animals receiving high dose treatment showed statistically significant ($p < 0.05$) decrease in glucose. The low and medium dose groups showed no statistically significant change (Fig. 11A).

- *Aspartate Aminotransferase (AST)*

Male animals receiving low, medium and high dose treatment showed significant ($p < 0.0001$, $p < 0.01$, $p < 0.001$) increase in AST (Fig. 11A). However, such changes were not evident in female animals (Fig. 11A).

- *Alkaline Phosphatase (ALP)*

Male animals receiving medium and high dose showed significant ($p < 0.001$) decrease in ALP (Fig. 11A).

- *Total protein*

Table 2
Summary of data relating to SARS-CoV-2 real-time PCR Ct value in the presence and absence of control and TSs.

E GENE- 48 h		Ct Mean							
S. No.	Sample Name	#1	#2	#3	Average CT	Delta CT	Fold change	wrt control	% Inhibi tion
1	DMSO	14.780	13.974	14.169	14.308	-0.000	1.000	100.000	-0.000
2	REMDE SIVIR	25.392	25.316	25.123	25.277	10.969	2004.441	0.050	99.950
3	E2	19.201	19.151	18.056	18.803	4.495	22.545	4.440	95.600
4	E4	24.554	23.495	23.325	23.791	9.483	715.690	0.140	99.900
5	E5	18.956	17.025	17.913	17.964	3.656	12.610	7.930	92.070
N GENE- 48 h		Ct Mean							
S. No.	Sample Name	#1	#2	#3	Average CT	Delta CT	Fold change	wrt control	% Inhibi tion
1	DMSO	15.165	14.322	14.659	14.715	0.000	1.000	100.000	0.000
2	REMDE SIVIR	24.895	24.801	24.419	24.705	9.990	1016.882	0.098	99.902
3	E2	18.673	18.251	17.897	18.274	3.559	11.785	8.500	91.500
4	E4	24.535	22.997	22.817	23.450	8.735	425.992	0.200	99.800
5	E5	18.290	16.666	17.300	17.418	2.703	6.514	15.350	84.648

CT: Cycle threshold; TS: Test sample.

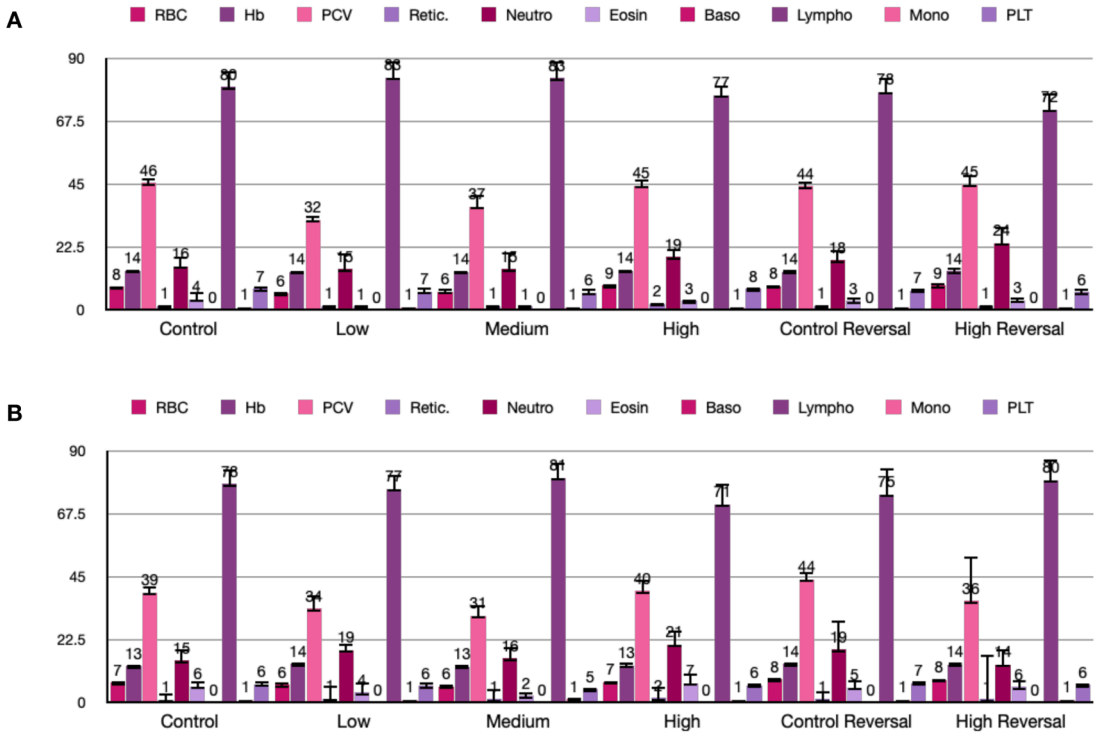

Fig. 10. A: Summary of group mean haematological estimations of male rats treated with different dos-es. **B:** Summary of group mean haematological estimations of female rats treated with different doses. (RBC: Red Blood Cell, Hb: Haemoglobin, PCV: Packed cell volume, Retic.: Reticulocytes, Neutro: Neu-trophils, Eosin: Eosinophils, Baso: Basophils, Lympho: Lymphocytes, Mono: Monocytes, PLT: Platelets).

Male and female animals receiving low, medium and high dose treatment showed statistically significant ($p < 0.05$) increase in total protein value (Fig. 11A and Fig. 11B**).**

- *Total cholesterol*

Male animals receiving low and medium dose treatment showed significant ($p < 0.05$) increase in total cholesterol (Fig. 11A**).**

- *Triglyceride*

Female animals receiving low and high dose treatment showed significant ($p < 0.05$) increase in triglyceride (Fig. 11B).

- *Blood Urea Nitrogen*

Female animals receiving medium dose treatment showed significant ($p < 0.01$) decrease in BUN (Fig. 11B).

- *Creatinine*

Male and female animals receiving low and medium dose treatment showed significant ($p<0.0001$) decrease in creatinine (Fig. 11A and Fig. 11B**).**

- *Total bilirubin*

Female animals receiving high dose treatment show significant ($p < 0.05$) decrease in total bilirubin (**Fig. 11B**).

- *Phosphorous*

Male animals receiving low dose treatment showed significant ($p < 0.01$) decreases in phosphorus (**Fig. 11B**).

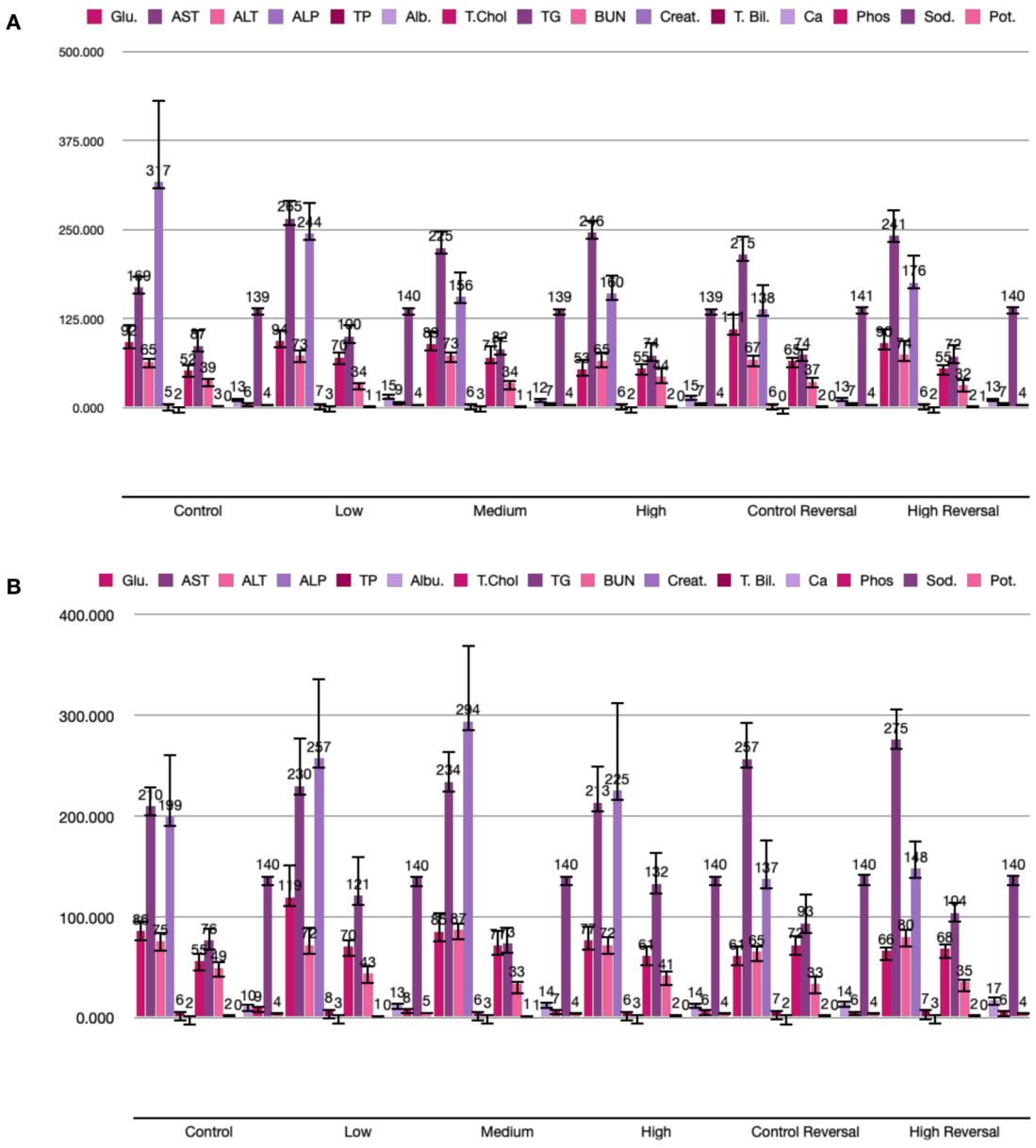

Fig. 11. **A:** Summary of group mean clinical chemistry estimations of male rats treated with different doses.. **B:** Summary of group mean clinical chemistry estimation of female rats treated with different dos-es. (Glu.: Glucose, AST: Aspartate aminotransferase, ALT: Alanine aminotransferase, ALP: Alkaline phos-phatase, TP: Total Protein, Albu.: Albumin, T.Chol.: Total cholesterol, TG: Triglyceride, BUN: Blood urea nitrogen, Creat.: Creatinine, T. Bill.: Total bilirubin, Ca: calcium, Phos: Phosphate, Sod.: Sodium, Pot.: Potassium).

Bone marrow analysis. Bone marrow analysis was conducted on day 29 and day 43. At low dose, treatment groups showed mild reactive plasmacytosis. At medium dose, treatment groups showed mild reactive myeloid hyperplasia. At high dose, treatment groups showed mild to moderate myeloid hyperplasia and mild reactive plasmacytosis. The control groups showed no bone marrow change. (Table 3**)**.

Urine analysis. Urine analysis showed no changes on day 29 and on day 43.

Organ weight. The organ weight comparison was done with control groups. Liver weight of male animals receiving high dose treatment showed significant ($p < 0.05$) decrease. Spleen of male animals receiving low dose and female animals receiving medium dose showed significant ($p < 0.05$) increase in weight. Lungs of female animals receiving medium dose showed significant ($p < 0.05$) decrease (**Table S2**).

For the rest of the organs (Kidneys, Heart, Brain, Testes and Adrenal) no changes in the weight was observed.

Histopathology. No histopathological changes were observed in the liver, kidney, and jejunum of animals treated with low, medium and high dose.

Conclusions

We have demonstrated that the *in vitro* anti-SARS-CoV-2 activity of plant extracts E4, E5, and E2, showed no cytotoxicity in VeroE6 cells. The IC_{50} study of extracts showed anti-SARS-CoV-2 activity of E4. The *in vivo* acute and sub-acute toxicity study of E 4.5.2 did not show any significant toxicity. Further, *in vivo* anti-SARS-CoV-2 activity needs to be demonstrated and worth investigating the test samples in clinical trials.

Table 3
Summary of bone marrow study performed in male and female animals treated with E 4.5.2 in sub-acute toxicity study.

Group (Dose in mg/kg)	Observation
GI (0.0)	All the six bone marrow smears from control group 6CM1 to 6CM6 show features suggestive of normal haematopoiesis. All the six bone marrow smears from the second control group 6CF1 to 6CF6 show features suggestive of normal haematopoiesis.
GII (200.0)	All the six bone marrow smears in the Low Dose group from 6LM1 to 6LM6 and 6LF1 to 6LF6 show features of mild reactive plasmacytosis. No pathological changes seen.
GIII (400.0)	All the six bone marrow smears in the medium dose group form 6MM1 to 6MM6 and 6MF1 to 6MF6 show features indicative of mild reactive myeloid hyperplasia. No specific pathological changes seen.
GIV (800.0)	All the six bone marrow smears in the high dose group from 6HM1 to 6HM6 and 6HF1 to 6HF6 show features of mild to moderate myeloid hyperplasia and mild reactive plasmacytosis. No specific pathological changes seen.
GV (0.0)	All the six bone marrow smears in the reversal control group 6CRM1 to 6CRM6 and 6CRF1 to 6CRF6 show features of normal haematopoiesis. No pathological changes seen.
GVI (800.0)	All the six bone marrow smears in the reversal high dose control group 6HRM1 to 6HRM6 and 6HRF1 to 6HRF6 show features indicative of normal haematopoiesis/ mild reactive plasmacytosi. No other haematopoitic abnormalities seen in any of these smears in the reversal groups.

Abbreviations: 6CM1- 6 control male 1, where 6 is total number of animals in group and 1 is an animal in group. CF- control female, LM- Low dose male, LF- Low dose female, MM- Medium dose male, LF- Medium dose female, HM- High dose male, HF- High dose female, CRM - Control reversible male, CRF - Control reversible female, HRM - High dose reversible male, HRF - High dose reversible female.

Author agreement statement

We the undersigned declare that this manuscript is original, has not been published before and is not currently being considered for publication elsewhere.

We confirm that the manuscript has been read and approved by all named authors and that there are no other persons who satisfied the criteria for authorship but are not listed. We further confirm that the order of authors listed in the manuscript has been approved by all of us.

We understand that the Corresponding Author is the sole contact for the Editorial process He/she is responsible for communicating with the other authors about progress. submissions of revisions and final approval of proofs

CRediT authorship contribution statement

Damle Latha: Conceptualization, Formal analysis, Funding acquisition, Methodology, Project administration, Validation, Writing – review & editing. **Damle Hrishikesh:** Conceptualization, Formal analysis, Funding acquisition, Methodology, Writing – review & editing. **Ganju Shiban:** Conceptualization, Funding acquisition, Writing – original draft, Writing – review & editing. **C Chandrashekar:** Investigation, Methodology. **BR Bharath:** Conceptualization, Data curation, Formal analysis, Investigation, Methodology, Resources, Software, Visualization, Writing – original draft, Writing – review & editing.

Declaration of Competing Interest

Latha Damle is the founder of Atrimed Biotech LLP and holds equity in Atrimed Pharmaceuticals. Shiban Ganju and Hrishikesh Damle hold equity shares in Atrimed Pharmaceuticals. Through this, authors declare that, there are no conflict of interest in publishing the manuscript entitled "In silico, *In vitro* Screening of Plant Extracts for Anti-SARS-CoV-2 Activity and Evaluation of Their Acute and Sub-Acute Toxicity" in phytomedicine journal.

Acknowledgement

Grant information: The study was sponsored by Atrimed Pharmaceuticals Pvt. Ltd and no external funding was received for the study.

Supplementary materials

Supplementary material associated with this article can be found, in the online version, at doi:10.1016/j.phyplu.2022.100233.

References

Balkrishna, A., Haldar, S., Singh, H., Roy, P., Varshney, A., 2021. Coronil, a tri-herbal formulation, attenuates spike-srotein-mediated SARS-CoV-2 viral entry into human alveolar epithelial cells and pro-inflammatory cytokines production by inhibiting spike protein-ace-2 interaction. J. Inflamm. Res. 14, 869–884.
Bhattacharya, S.K., Muruganandam, A.V., 2003. Adaptogenic activity of Withania somnifera: an experimental study using a rat model of chronic stress. Pharmacol. Biochem. Behav. 75, 547–555.
Caceres, D.D., Hancke, J.L., Burgos, R.A., Wikman, G.K., 1997. Prevention of common colds with Andrographis paniculata dried extract. A Pilot double Blind Trial. Phytomed. 4, 101–104.
Caly, L., 2020. The FDA-approved drug ivermectin inhibits the replication of SARS-CoV-2 *in vitro*. Antivir. Res. 178, 104787.
Chandrasekhar, K., Kapoor, J., Anishetty, S., 2012. A prospective, randomized double-blind, placebo-controlled study of safety and efficacy of a high-concentration full-spectrum extract of ashwagandha root in reducing stress and anxiety in adults. Indian J. Psychol. Med. 34, 255–262.
Choi, H.J., 2016. Evaluation of antiviral activity of Zanthoxylum species against picornaviruses. Osong Public Health Res. Perspect 6, 400–403.
Choi, H.J., Song, J.H., Kwon, D.H., 2008. Antiviral activity of Zanthoxylum species against influenza virus. Korean J. Med. Crop Sci. 16, 273–278.
Chopra, R.N., Nayar, S.L., Chopra, I.C., 1986. Glossary of Indian medicinal plants. New Delhi: Council of Sci. Ind. Res. 1, 51–83.
Diwan, P.C., Karwande, I., Singh, A.K., 1991. Anti-anxiety profile of mandukparni Centella asiatica Linn in animals. Fitoterapia 62, 255–257.
Douangamath, A., Fearon, D., Gehrtz, P., Krojer, T., Lukacik, P., Owen, C.D., Resnick, E., Strain-Damerell, C., Aimon, A., Abranyi-Balogh, P., Brandao-Neto, J., Carbery, A., Davison, G., Dias, A., Downes, T.D., Dunnett, L., Fairhead, M., Firth, J.D., Jones, S.P., Keeley, A., Keseru, G.M., Klein, H.F., Martin, M.P., Noble, M.E.M., O'Brien, P., Powell, A., Reddi, R.N., Skyner, R., Snee, M., Waring, M.J., Wild, C., London, N., von Delft, F., Walsh, M.A., 2020. Crystallographic and electrophilic fragment screening of the SARS-CoV-2 main protease. Nat. Commun. 11, 5047.
Jin, Z., Du, X., Xu, Y., Deng, Y., Liu, M., Zhao, Y., Zhang, B., Li, X., Zhang, L., Peng, C., Duan, Y., Yu, J., Wang, L., Yang, K., Liu, F., Jiang, R., Yang, X., You, T., Liu, X., Yang, X., Bai, F., Liu, H., Liu, X., Guddat, L.W., Xu, W., Xiao, G., Qin, C., Shi, Z., Jiang, H., Rao, Z., Yang, H., 2020. Structure of Mpro from SARS-CoV-2 and discovery of its inhibitors. Nature 582, 289–293.
Kashman, Y., Gustafson, K.R., Fuller, R.W., Cardellina, J.H., McMahon, J.B., Currens, M. J., Buckheit, R.W., et al., 1992. The calanolides, a novel HIV-inhibitory class of coumarin derivatives from the tropical rainforest tree, Calophyllum lanigerum. J. Med. Chem. 35, 2735–2743.
Kashyap, V.K., Dhasmana, A., Yallapu, M.M., Chauhan, S.C., Jaggi, M., 2020. Withania somnifera as a potential future drug molecule for COVID-19. Future Drug Discov. 2, FDD50.
Kulkarni, S.K., Dhir, A., 2008. Withania somnifera: an Indian ginseng. Prog Neuro-Psychopharmacol. Biol. Psychiatry 32, 1093–1105.
Laure, F., Raharivelomanana, P., Butaud, J.F., Bianchini, J.P., Gaydou, E.M., 2008. Screening of anti-HIV-1 inophyllums by HPLC–DAD of Calophyllum inophyllum leaf extracts from French Polynesia Islands. Anal. Chim. Act. 624, 147–153.
Melchior, J., Palm, S., Wikman, G., 1997. Controlled clinical study of standardized Andrographis paniculata extract in common cold a pilot trial. Phytomedicine 3, 315–318.
Melchior, J., Spasov, A.A., Ostrovskij, O.V., Bulanov, A.E., Wikman, G., 2000. Double blind, placebo-controlled pilot and phase III study of activity of standardized Andrographis paniculata Herba Nees extract fixed combination (Kan jang) in the treatment of uncomplicated upper-respiratory tract infection. Phytomedicine 7, 341–350.
Pant, M., Ambwani, T., Umapathi, V., 2012. Antiviral activity of Ashwagandha extract on infectious bursal disease virus replication. Ind. J. Sci. Tech. 5, 2750–2751.
Poolsup, N., Suthisisang, C., Prathanturarug, S., Asawamekin, A., Chanchareon, U., 2004. Andrographis paniculata in the symptomatic treatment of uncomplicated upper respiratory tract infection: systematic review of randomized controlled trials. J. Clin. Pharm. Ther. 29, 37–45.
Provino, R., 2010. The role of adaptogens in stress management. Aust. J. Med. Herbal. 22, 41–49.

Richman, D.D., Nathanson, N., 2016. Antiviral Therapy. Viral Pathogenesis. 1, 271–287.
Saxena, R.C., Singh, R., Kumar, P., Yadav, S.C., Negi, M.P.S., Saxena, V.S., Joshua, A.J., Vijayabalaji, V., Goudar, K.S., Venkateshwarlu, K., Amit, A., 2010. A randomized double blind placebo controlled clinical evaluation of extract of Andrographis paniculata (KalmColdTM) in patients with uncomplicated upper respiratory tract infection. Phytomedicine 17, 178–185.
Sharma, V., Sharma Pracheta, S., Paliwal, R., 2011. Withania somnifera: a rejuvenating ayurvedic medicinal herb for the treatment of various human ailments. Int. J. PharmTech. Res. 3, 187–192.
Singh, G., Sharma, P.K., Dudhe, R., Singh, S., 2010. Biological activities of Withania somnifera. Ann. Biol. Res. 1, 56–63.
Sun, B., Wu, L., Wu, Y., Zhang, C., Qin, L., Hayashi, M., Kudo, M., Gao, M., Liu, T., 2020. Therapeutic potential of Centella asiatica and its triterpenes: a Review. Front. Pharmacol. 11, 1–24.
Tan, E.L., Ooi, E.E., Lin, C.Y., et al., 2004. Inhibition of SARS coronavirus infection *in vitro* with clinically approved antiviral drugs. Emerg. Infect. Dis. 10, 581–586.
Tan, M.C., Oyong, G.G., Shen, C.C., Ragasa, C.Y., 2017. Cytotoxic labdane diterpenoids from Andrographis paniculata (Burm.F) Nees. Asian J. Pharma Clin. Res. 10, 99–104.
Thamlikitkul, V., Dechatiwongse, T., Theerapong, S., et al., 1991. Efficacy of Andrographis paniculata, Nees for pharyngotonsillitis in adults. J. Med. Assoc. Thai. 74, 437–442.
Tilahun, A., Dinkenesh, C., Netsanet, F., Dawit, S., Tesfaye, S., Asfaw, D., Beyene, P., 2020. Evaluation of acute and sub-acute toxicity of selected traditional antiurolithiatic medicinal plant extracts in wistar albino rats. Toxicol. Rep. 7, 1356–1365.
Vaux, D.L., Fidler, F., Cumming, G., 2012. Replicates and repeats–what is the difference and is it significant? A brief discussion of statistics and experimental design. EMBO Rep. 13, 291–296.
Wan, Y., Shang, J., Graham, R., Baric, R.S., Li, F., 2020. Receptor recognition by novel coronavirus from Wuhan: an analysis based on decade-long structural studies of SARS. J. Virol. e00127-20.
Yin, W., Mao, C., Luan, X., Shen, D.D., Shen, Q., Su, H., Wang, X., Zhou, F., Zhao, W., Gao, M., Chang, S., Xie, Y.C., Tian, G., Jiang, H.W., Tao, S.C., Shen, J., Jiang, Y., Jiang, H., Xu, Y., Zhang, S., Zhang, Y., Xu, H.E., 2020. Structural basis for inhibition of the RNA-dependent RNA polymerase from SARS-CoV-2 by remdesivir. Science 1499–1504.
Yoosook, C., Bunyapraphatsara, N., Boonyakiat, Y., Kantasuk, C., 2000. Anti-herpes simplex virus activities of crude water extracts of Thai medicinal plants. Phytomedicine 6, 411–419.